2023

Sensitivity of the Relationship Between Antarctic Ice Shelves and Iron Supply to Projected Changes in the Atmospheric Forcing

Michael S. Dinniman
Old Dominion University, mdinnima@odu.edu

Pierre St-Laurent
Old Dominion University, pierre@ccpo.odu.edu

Kevin R. Arrigo

Eileen E. Hofmann
Old Dominion University, ehofmann@odu.edu

Gert L. van Dijken

Original Publication Citation

Dinniman, M. S., St-Laurent, P., Arrigo, K. R., Hofmann, E. E., & van Dijken, G. L. (2023). Sensitivity of the relationship between Antarctic ice shelves and iron supply to projected changes in the atmospheric forcing. *Journal of Geophysical Research: Oceans*, 128(2), 1-18, Article e2022JC019210. https://doi.org/10.1029/2022JC019210

JGR Oceans

RESEARCH ARTICLE
10.1029/2022JC019210

Key Points:

- Projected atmospheric changes increased ice shelf basal melt in a circum-Antarctic ocean/sea ice/ice shelf circulation model
- Surface dissolved iron supply, including from sediments, increased but the ice shelf melt effect on the supply was spatially heterogeneous
- Summer sea ice decreased and summer mixed layers shoal suggesting a possible reduction in nutrient and light limitation

Supporting Information:

Supporting Information may be found in the online version of this article.

Correspondence to:

M. S. Dinniman,
msd@ccpo.odu.edu

Citation:

Dinniman, M. S., St-Laurent, P., Arrigo, K. R., Hofmann, E. E., & van Dijken, G. L. (2023). Sensitivity of the relationship between Antarctic ice shelves and iron supply to projected changes in the atmospheric forcing. *Journal of Geophysical Research: Oceans*, *128*, e2022JC019210. https://doi.org/10.1029/2022JC019210

Received 18 AUG 2022
Accepted 4 FEB 2023

Sensitivity of the Relationship Between Antarctic Ice Shelves and Iron Supply to Projected Changes in the Atmospheric Forcing

Michael S. Dinniman[1], Pierre St-Laurent[1,2], Kevin R. Arrigo[3], Eileen E. Hofmann[1], and Gert L. van Dijken[3]

[1]Center for Coastal Physical Oceanography, Old Dominion University, Norfolk, VA, USA, [2]Virginia Institute of Marine Science, William & Mary, Gloucester Point, VA, USA, [3]Department of Earth System Science, Stanford University, Stanford, CA, USA

Abstract Upward advection or mixing of iron-rich deep waters due to circulation changes driven by the rate of basal ice shelf melt was shown to be a primary control on chlorophyll *a* production in coastal polynyas over the Antarctic continental shelf. Here, the effects of atmospheric changes projected in 2100 on this relationship were examined with a 5-km resolution ocean/sea ice/ice shelf model of the Southern Ocean with different simulated dissolved iron sources and idealized biological uptake. The atmospheric changes are added as idealized increments to the forcing. Inclusion of a poleward shift and strengthening of the winds, increased precipitation, and warmer atmospheric temperatures resulted in doubling of the heat advected onto the continental shelf and an 83% increase in the total Antarctic ice shelf basal melt. The total dissolved iron supply to the surface waters over the continental shelf increased by 62%, while the surface iron supply due just to basal melt driven overturning increased by 48%. However, even though the ice shelf driven contribution becomes less important to the total iron supply on average (29% of total), the ice shelf involvement becomes relatively even more important in some locations, such as the Amundsen and Bellingshausen Seas. The modified atmospheric conditions also produced a reduction in summer sea ice extent and a shoaling of the summer mixed layers. These simulated responses to projected changes suggest relief of light and nutrient limitation for phytoplankton blooms over the Antarctic continental shelf and perhaps an increase in annual production in years to come.

Plain Language Summary The growth of phytoplankton in Antarctic coastal waters is limited by the availability of light for photosynthesis and the supply of the trace nutrient dissolved iron. When the bottom of the floating margins of the Antarctic ice sheet (the ice shelves) melts, the melt water is less dense and rises along the base of the ice shelf, which causes deeper waters with high iron concentrations to rise toward the surface. An earlier study showed that this overturning circulation driven by the melting ice shelves is an important source of dissolved iron to the well-lit surface waters in many locations around Antarctica. In this study, a computer model of the ocean and ice shelves is forced with projected future changes in different atmospheric conditions. These changes in the atmosphere lead to an increase in the ice shelf melt, the dissolved iron supplied to the ocean surface due to overturning driven by the ice shelf melt, and the total dissolved iron supplied to the surface. The atmospheric changes also reduce the summer sea ice cover, making more light available to the ocean surface. All these changes suggest that in the future, phytoplankton growth around Antarctica will increase.

1. Introduction

Phytoplankton growth and abundance in the waters around Antarctica, including over the continental shelf, is limited by the availability of light and trace metals, primarily dissolved iron (dFe) (Boyd, 2002; Boyd et al., 2012; De Baar et al., 1990; Martin et al., 1990). Concentrations of dFe in Antarctic shelf waters are generally insufficient to promote complete utilization of macronutrients by phytoplankton (Arrigo et al., 2000; Mills et al., 2012; W. O. Smith & Gordon, 1997). This limitation on growth is due to the low dFe supply rate to Antarctic surface waters, which was generally considered to be restricted to sources provided by sediment resuspension, sea ice melt, and input from melting glaciers (Arrigo et al., 2015; Boyd et al., 2012). Although dFe sources are more diverse on the continental shelf than for the Southern Ocean, deep sources such as shelf sediments require a physical mechanism such as vertical mixing to supply the surface water.

Arrigo et al. (2015) examined the relative importance of several environmental variables in supporting chlorophyll *a* concentrations and rates of net primary production estimated from satellite-based observations for 46 coastal polynyas around Antarctica. This analysis found that ice shelf basal melt rates explained 59% of the between-polynya variance in mean chlorophyll *a* concentration and explained twice as much of the variance as the next most important variable, thus suggesting that the productivity of coastal polynyas is sensitive to the release of dFe from melting ice shelves. Basal melting of ice shelves can drive a buoyancy-forced overturning circulation within ice shelf cavities (Greisman, 1979) that can significantly modify the circulation outside the ice shelf cavity (Jourdain et al., 2017). St-Laurent et al. (2017) found that for the Amundsen Sea polynya, this overturning circulation supplied significantly more dFe from deep sources on the shelf, such as Circumpolar Deep Water (CDW) intrusions or sediments, to the surface waters outside the cavity than directly supplied by dFe in the ice shelf meltwater (see also Twelves et al., 2021). Dinniman et al. (2020) analyzed ice shelf basal melt and its effect on coastal circulation for the entire Antarctic continental shelf and showed that this overturning circulation is an important component of the total dFe supply over much of the shelf. For some shelf regions, such as the Amundsen Sea, the overturning circulation was the primary mechanism for transporting deep sources of dFe to the surface.

Two relatively well observed locations on the Antarctic continental shelf provide examples of contrasting sources of dFe supply and the role of local physics in changing this supply. The eastern Amundsen Sea has high ice shelf melt (Adusumilli et al., 2020; Depoorter et al., 2013; Liu et al., 2015; Rignot et al., 2013), with observations of relatively large amounts of ice shelf meltwater (Biddle et al., 2017, 2019; Randall-Goodwin et al., 2015) and winter mixed layers that do not extend all the way through the subsurface CDW layer (Mallett et al., 2018). The primary sources of dFe supply to the surface in the eastern Amundsen are thought to be local iron recycling (Gerringa et al., 2020) and sediment supply that gets to the surface via ice shelf melt driven overturning (St-Laurent et al., 2017). Conversely, the western Ross Sea has relatively weak ice shelf melt (Adusumilli et al., 2020; Depoorter et al., 2013; Liu et al., 2015; Rignot et al., 2013) and deep winter vertical mixing that can extend through the entire water column in some areas (Piñones et al., 2019; Yoon et al., 2020). The primary sources of dFe surface supply in this region are thought to be via sea ice melt and sediment supply that is transported to the surface without the contribution of ice shelf overturning (Mack et al., 2017; McGillicuddy et al., 2015; Salmon et al., 2020).

Coupled Model Intercomparison Project Phase 5 (CMIP5) (Taylor et al., 2012) high emissions scenario (RCP8.5) simulations project a strengthening and poleward shift in the mean Southern Hemisphere westerlies (Bracegirdle et al., 2018; Simpson & Polvani, 2016; Spence et al., 2014; Wilcox et al., 2012), an increase in the precipitation over the Antarctic continent and high latitude Southern Ocean (Behrangi & Richardson, 2018; Palerme et al., 2017), and an increase in air temperature over the Southern Ocean and the Antarctic continent (Barthel et al., 2020; Behrangi & Richardson, 2018; Bracegirdle et al., 2018). A manifestation of these projected changes is increased simulated primary production over the Antarctic continental shelf by 2100 due to enhanced iron supply and greater light availability from the accelerated seasonal melting of sea ice (Cabré et al., 2014; Hauck et al., 2015; Leung et al., 2015). Results from the Coupled Model Intercomparison Project Phase 6 (CMIP6) high emissions scenarios showed similar changes in the high southern latitudes (Kwiatkowski et al., 2020). However, neither the CMIP5 nor the CMIP6 models include ice shelf processes and it has been shown that adding glacial meltwater can produce significant changes in the simulated physics and biogeochemistry in the Antarctic (Bronselaer et al., 2020; Jeong et al., 2020). Ocean models and Earth System Models with biogeochemical sub-models that include parameterizations for dFe supply from glacial ice, without explicit simulation of ice shelf/ocean interactions, show significantly increased primary production over the Antarctic continental shelf and near shelf regions of the Southern Ocean when the glacial iron supply is added (Death et al., 2014; Laufkötter et al., 2018; Person et al., 2019, 2021).

The objective of this study is to assess the responses of Antarctic ice shelves and shelf waters, and subsequent dFe supply to the surface waters over the Antarctic continental shelf, that are produced by projected changes in wind location and intensity, and increased precipitation and atmospheric temperature. The projected changes in atmospheric forcing are based on CMIP5 projections over and near Antarctica for 2100 and are imposed as incremental changes to the forcing fields used with a primitive equation ocean/sea ice/ice shelf circulation model of the Southern Ocean (Dinniman et al., 2020).

2. Model and Simulations

2.1. Circum-Antarctic Model Structure

The circum-Antarctic circulation model used in this study, described in Dinniman et al. (2020), is based on the Regional Ocean Modeling System (ROMS), which is a primitive equation finite volume model with a terrain following vertical coordinate system (Haidvogel et al., 2008; Shchepetkin & McWilliams, 2009). The model includes a dynamic sea-ice model (Budgell, 2005), and the mechanical and thermodynamic interactions between floating ice shelves and the water underneath are explicitly simulated.

As described in Dinniman et al. (2020), the model domain includes the entire Antarctic continental shelf, including the portion (~35%) of the continental shelf ocean underneath the floating ice shelves, and extends northward from the continent past the annual maximum sea ice extent and across Drake Passage to South America (Figure 1). The model grid uses a polar stereographic projection with a 5-km horizontal resolution. The 32 terrain-following vertical levels have smaller spacing near the surface and bottom with a mean thickness of 1.69 m for the surface level over the open Antarctic continental shelf (1.22 m underneath an ice shelf). The bathymetry for the ocean and ice shelf cavities (bottom and top ocean surfaces) is from the RTopo-2 data set (Schaffer et al., 2016), with updates in the Amundsen Sea Embayment (Millan et al., 2017).

The modeled ice shelves are assumed to be static, with no changes in ice shelf thickness or extent and no iceberg calving over the sub-decadal time scales of the simulations. The model explicitly simulates mechanical (surface drag and depressed ocean free surface) and thermodynamic (heat and salt fluxes due to ice melting and freezing) interactions between the floating ice shelves and the water underneath (Dinniman et al., 2011; D. M. Holland & Jenkins, 1999). The dynamic sea-ice model (Budgell, 2005) includes two-layer ice thermodynamics (Häkkinen & Mellor, 1992; Mellor & Kantha, 1989), a snow layer, a simple estimate of frazil ice production (Steele et al., 1989), and an elastic-viscous-plastic rheology (Hunke, 2001; Hunke & Dukowicz, 1997). The open ocean momentum, heat, and fresh water (imposed as a salt flux) fluxes and vertical momentum and tracer mixing are as described in Dinniman et al. (2020). Ocean tides are not included.

The circum-Antarctic simulation used in this study starts after a 6-year model spin-up. Lateral boundary conditions for temperature and salinity (using data from the World Ocean Atlas 2009 (Locarnini et al., 2010)), velocity (with depth averaged values from the Simple Ocean Data Assimilation (SODA, version 1.4.2) ocean reanalysis (Carton & Giese, 2008)), and sea surface height (also from SODA) are the same as in Dinniman et al. (2015, 2020). There is no need to specify sea ice boundary information as the model domain totally encompasses any sea ice observed during the satellite era (1979 to present). Following the 6-year spin-up simulation, the model was run for 7 years using atmospheric forcing for winds, 2-m air temperatures, sea level pressure, and relative humidity obtained from the ERA-Interim reanalysis (Dee et al., 2011). Precipitation and cloud fraction were specified as described in Dinniman et al. (2020). The atmospheric forcing conditions were from 2010, and the simulation was forced (6 year spin-up and 7 year run) by continuously repeating 2010 conditions to assess model drift and externally forced variability in producing interannual changes in the simulated circulation (**Base** simulation: see Section 2.3 and Table 2 below).

2.2. Tracers

As in Dinniman et al. (2020), 14 independent numerical tracers were used to simulate the input of different dFe sources to Antarctic continental shelf waters (Table 1). Eight tracers, initialized in different sectors of the Antarctic Ice Sheet (Table 1, Figure 1), were used to track glacial meltwater. The simulated meltwater concentration is converted to dFe concentration using an end member value of 20 nM, which is within the range of dFe estimates for glacial meltwater (20–50 nM, Gerringa et al., 2012; 29 ± 21 nM, McGillicuddy et al., 2015; 22 nM, St-Laurent et al., 2017; 71 ± 121 nM, Forsch et al., 2021). The simulated dFe concentration in a model grid cell is then determined by the product of the glacial meltwater fraction and the end member concentration. Inputs of glacial meltwater derived from iceberg melt or grounded land ice melt that advects to the open ocean through subglacial hydrology (e.g., Death et al., 2014) were not included in the simulations.

The inputs of dFe from Antarctic continental shelf sediments were tracked with two tracers (Table 1). The dFe flux from sediments into the bottom waters over the Antarctic continental shelf is difficult to estimate because of the lack of observational data. However, near-bottom profiles of dFe concentration are available for some shelf areas in Antarctica. Thus, the approach of Mack et al. (2017) was used in which the dFe concentration in

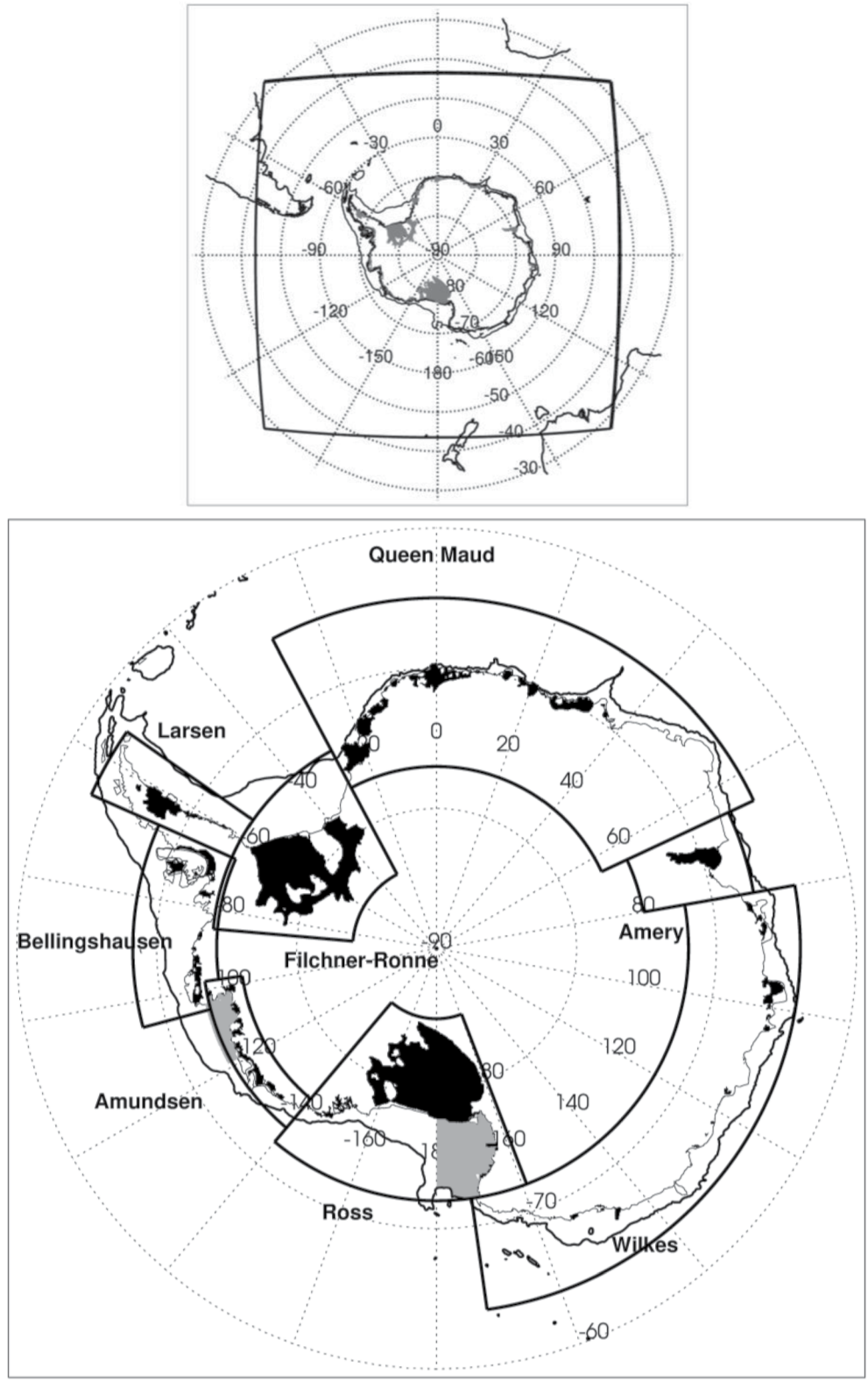

Figure 1. (Top panel) Map showing the extent of the circum-Antarctic model domain (outer solid line) and floating ice shelves (gray shaded areas) included in the model. (Bottom panel) Expanded view of the model domain over the Antarctic continental shelf showing the eight sectors used for the ice shelf melt water tracers (black solid lines). The ice shelves included in the model (black shaded areas) and the western Ross Sea and eastern Amundsen Sea continental shelf areas used for simulation analysis (gray shaded areas) are shown. The 1,200-m isobath is also shown (thin black line).

Table 1
Sources of Dissolved Iron (dFe) Used in the Tracer Simulation

Tracer designation	Tracer source	Tracer location
dFe_{IS1}	Ice shelf melt	Ross Sector
dFe_{IS2}	Ice shelf melt	Amundsen Sector
dFe_{IS3}	Ice shelf melt	Bellingshausen Sector
dFe_{IS4}	Ice shelf melt	Larsen Sector
dFe_{IS5}	Ice shelf melt	Filchner-Ronne Sector
dFe_{IS6}	Ice shelf melt	Queen Maud Sector
dFe_{IS7}	Ice shelf melt	Amery Sector
dFe_{IS8}	Ice shelf melt	Wilkes Sector
dFe_{SED}	Sediments	
dFe_{SED_ZC}	Sediments	Reduced in ice shelf cavities
dFe_{CDW}	Circumpolar Deep Water	
dFe_{CDW_ZC}	Circumpolar Deep Water	Reduced in ice shelf cavities
dFe_{SI}	Sea ice melt	
dFe_{SI_ZC}	Sea ice melt	Reduced in ice shelf cavities

Note. The region included in each ice shelf melt sector is shown in Figure 1. Tracers that are reduced in the ice shelf cavity are indicated by ZC (see text for details).

the lowest level of the model over the continental shelf was set to a constant value (0.35–2.05 nM depending on the bottom depth) based on the observed profiles (Dinniman et al., 2020). The sediment tracer was initialized to zero everywhere in the model domain above the bottom layer and was then nudged (in the bottom layer only) to the pre-determined value with a timescale of 10 days. The tracer value in the bottom layer of the model is continuously nudged to the estimated sediment concentration during the entire simulation, but can freely advect and diffuse throughout the rest of the water column. The first sediment tracer (dFe_{SED}) was free to advect and diffuse over the entire model domain. The second (dFe_{SED_ZC}) was relaxed to zero (time scale of 10 days) within ice shelf cavities to remove the cavity influence on the tracer without changing the model circulation dynamics (St-Laurent et al., 2017).

Inputs of dFe by CDW (Table 1) were simulated with two tracers (Table 1) that were initialized with zero concentration over the entire continental shelf (defined by the 1,200-m isobath and including ice shelf cavities) and a value of 1 in off-shelf CDW water. Similar to the sediment tracers, one CDW tracer (dFe_{CDW}) was free to advect and diffuse over the entire model domain, and the second (dFe_{CDW_ZC}) was relaxed to zero (timescale of 10 days) within any ice shelf cavity. The CDW tracer concentration was related to dFe using an end member concentration of 0.32 nM, which is an average of measured CDW dFe concentrations just off the Antarctic continental shelf (McGillicuddy et al., 2015; Seyitmuhammedov et al., 2022; Sherrell et al., 2015; A. J. R. Smith et al., 2021).

The supply of dFe from melting sea ice was assessed with two tracers (Table 1). Both sea ice melt tracers are initialized with zero concentration. The removal of dFe from the surface water during the growth of sea ice (e.g., Lannuzel et al., 2016) was not explicitly represented in the simulations, only its net effect (see below). One sea ice meltwater tracer (dFe_{SI}) advects and diffuses over the entire model domain; the second (dFe_{SI_ZC}) is relaxed to zero (timescale of 10 days) within any ice shelf cavity. The sea ice melt tracer concentration is related to dFe concentration using an end member value of 5.0 nM representing the net effect of iron incorporation into sea ice. Lannuzel et al. (2016) show a large range (0.1–110 nM) in measured concentrations of dFe in Antarctic sea ice, and the value of 5.0 nM is consistent with their median value of 4.4 nM. The tracers do not include dFe inputs from other sources, such as Aeolian deposition, hydrothermal vents, and glacial meltwater from icebergs and the grounded ice sheet (Dinniman et al., 2020).

The different tracers freely advect and diffuse over the model continental shelf for the first 4 years and 11 months of the simulation at which point the surface concentrations approached an annual steady state (Figure S1 in Supporting Information S1). In December of the fifth year of the simulation, tracer concentrations in the upper water column were reduced to simulate biological uptake as in Dinniman et al. (2020). From 1 December through 28 February of the next 2 years of simulation (years 5/6 and 6/7), biological uptake was included by relaxing all tracers to zero in the upper 100 m of the water column with a timescale of 30 days in the upper 50 m and 60 days for 50–100 m. The depth dependence of the uptake was a simple parameterization for variations in light conditions, but the impact of using uniform depths remains to be investigated with further experiments. The

Table 2
Summary of Simulations

Simulation	Winds	Precipitation	Atmospheric temperature
Base	ERA-Interim	GPCP	ERA-Interim
Winds	ERA-Interim × 1.15 + 4°S shift	GPCP	ERA-Interim
Winds + Precip	ERA-Interim × 1.15 + 4°S shift	GPCP × 1.2	ERA-Interim
All	ERA-Interim × 1.15 + 4°S shift	GPCP × 1.2	ERA-Interim +2.5°C

Note. The Global Precipitation Climatology Project (GPCP) is described in Adler et al. (2003). See text for details.

"biological uptake" was not applied underneath the ice shelves, but was active under the sea ice. Note that this is a simplification from reality as some areas remain ice covered throughout the austral summer, and light limitation under sea ice would normally reduce the uptake taking place there. Over the same time periods, dFe scavenging, which limits excessive dFe accumulation in the lower portion of the water column, was approximated by relaxing tracer concentrations throughout the entire water column toward zero with a timescale of 10^3 days (Dutkiewicz et al., 2005).

2.3. Simulations

The analysis of projected atmospheric changes on dFe provisioning to the Antarctic continental shelf was done using a base simulation and three perturbation simulations (Table 2). The **Base** simulation, described above, is the same as that used by Dinniman et al. (2020). The three perturbation simulations used idealized changes to the atmospheric forcing based on the CMIP5 projections for 2100 of the atmospheric conditions over the Antarctic continent and Southern Ocean as follows.

For the first perturbation simulation (**Winds**, Table 2), the ERA-Interim winds from the northern model boundary to 70°S were shifted 4° poleward and both components of the wind were increased by 15% north of 70°S (Donat-Magnin et al., 2017; Spence et al., 2014), as suggested by analyses of changes in the southern hemisphere westerlies in the RCP8.5 CMIP5 projections (Spence et al., 2014). Palerme et al. (2017) showed a 24% increase in the mean precipitation over the Antarctic continent in the CMIP5 RCP8.5 projections out to 2100 while Behrangi and Richardson (2018) found a 19% increase in precipitation over the high latitude Southern Hemisphere (55–82.5°S) for the same simulations. Based on these analyses, the second perturbation simulation (**Winds + Precip**, Table 2) added a constant 20% increase in the atmospheric precipitation, simulated as rain or snow depending on the atmospheric temperature, to the modified wind forcing. Atmospheric surface temperatures are projected to increase by 2°C–3°C over the Southern Ocean (Behrangi & Richardson, 2018; Bracegirdle et al., 2018) and the Antarctic continent (Barthel et al., 2020) by 2100 based on CMIP5 RCP8.5 simulations. The third perturbation simulation (**All**, Table 2) included a uniform 2.5°C increase in atmospheric temperatures. For the three modified forcing simulations, the changed atmospheric forcing was applied at the end of the 6-year spin-up and the simulations were run for the same 7-year period used for the **Base** simulation.

3. Model Results

3.1. Melt Rate

The total simulated annual average ice shelf basal melt rate around the entire continent for the **Base** simulation was 833 Gt yr^{-1} (Table 3), which is lower than recent estimates of 1,000–1,600 Gt yr^{-1} for the total melt around Antarctica (Adusumilli et al., 2020; Depoorter et al., 2013; Liu et al., 2015; Rignot et al., 2013). The difference in simulated and observed melt is attributable to under-estimates of the melting for some of the warm water ice shelves in the Amundsen Sea (Dinniman et al., 2020) and the considerable temporal variability in observed annual average melt rates, for example, the 400 Gt yr^{-1} decrease between 2009 and 2018 shown by Adusumilli et al. (2020). Also, the model configuration does not resolve several small (<100 km^2) ice shelves (Dinniman et al., 2015).

A poleward shift in winds accompanied by strengthening led to a 50% increase in the total ice shelf basal melt rate (**Winds**: 1,253 Gt yr^{-1}), with changes being heterogeneously distributed around the continent (Table 3; Figure S2 in Supporting Information S1). The melt rate more than doubled underneath the ice shelves near the dateline (Brunt, Riiser-Larsen, Fimbul, Jelbart). Melt rate decreased under the Pine Island Glacier Ice Shelf, but increased for the Getz Ice Shelf as well as most of the other Amundsen area ice shelves. Increased precipitation did not significantly change the total basal melt rate (**Winds + Precip**: 1,265 Gt yr^{-1}), but basal melt rate was altered for specific ice shelves such as Getz and Pine Island (Table 3). Increased air temperature produced a 21% increase in the basal melt rate (**All**: 1,528 Gt yr^{-1}), with significant increases over much of the Amundsen Sea, especially Pine Island Ice Shelf (Table 3; Figure S3 in Supporting Information S1). Changes in the wind forcing may have an influence farther down into the water column than changes in the atmospheric temperatures and, as also shown in Dinniman et al. (2018), this is reflected in the basal melt. Most (62%) of the increase in the basal melt rate due to wind changes occurred below 100 m. In contrast, most of the change in the basal melt rate produced by increasing air temperature occurred higher in the water column (61% of the increase between **All** and **Winds + Precip** is

Table 3
Simulated Basal Melt Rates for the Entire Continent (Total: Gt yr^{-1}) and the Larger Antarctic Ice Shelves (m yr^{-1}) From the Four Simulations (Table 2)

Ice shelf (sector)	Base Gt yr^{-1}; m yr^{-1}	Winds Gt yr^{-1}; m yr^{-1}	Winds and precip Gt yr^{-1}; m yr^{-1}	All Gt yr^{-1}; m yr^{-1}
Total	833	1,253	1,265	1,528
Amery (Amery)	0.61 ± 0.24	0.74 ± 0.32	0.74 ± 0.31	0.96 ± 0.56
Ross (Ross)	0.22 ± 0.08	0.23 ± 0.08	0.24 ± 0.08	0.28 ± 0.13
Getz (Amundsen)	3.14 ± 1.04	4.04 ± 0.67	4.58 ± 0.60	4.79 ± 1.11
Pine Island (Amundsen)	6.77 ± 1.13	4.11 ± 2.81	5.29 ± 2.40	7.77 ± 1.68
Abbot (Bellingshausen)	0.94 ± 0.27	1.73 ± 0.34	1.69 ± 0.32	1.59 ± 0.38
George VI (Bellingshausen)	3.80 ± 0.50	5.39 ± 0.54	5.58 ± 0.57	5.67 ± 0.67
Larsen C (Larsen)	0.48 ± 0.14	0.68 ± 0.25	0.70 ± 0.25	0.92 ± 0.41
Filchner-Ronne (Filchner-Ronne)	0.24 ± 0.03	0.29 ± 0.03	0.28 ± 0.03	0.21 ± 0.04
Brunt + Riiser-Larsen (Queen Maud)	0.50 ± 0.33	1.14 ± 0.81	1.06 ± 0.79	1.32 ± 0.98
Fimbul + Jelbart (Queen Maud)	1.23 ± 0.75	2.88 ± 1.42	2.87 ± 1.46	3.65 ± 2.26

Note. The ice shelf sector (Figure 1) corresponding to each ice shelf is given. The range shown for the simulated melt rates is the standard deviation of the 5-day averages, which mostly reflects seasonal variability.

above 100 m). The combined effect of the modified atmospheric forcing fields resulted in an 83% increase in the total basal melt rate with significant increases everywhere, except for a few locations including the two large cold water ice shelves, the Ross and Filchner-Ronne Ice Shelves (Table 3; Figure 2).

3.2. Heat Budget

The annual mean temperature over the continental shelf (defined by the 1,200-m isobath) was approximately in steady-state over the last two years of all simulations. This implies that the change in heat for the entire water column is essentially zero, meaning there is a balance between the heat advected onto the continental shelf and the heat lost through the surface (Dinniman et al., 2015) to either the atmosphere, which can lead to a net production of sea ice over the Antarctic continental shelf (P. R. Holland & Kwok, 2012; Petty et al., 2014), or the melting of glacial ice. Heat budget changes were calculated for the model domain using results from the four simulations. The heat budgets for the Antarctic continental shelf (Table 4) showed that a poleward shift and intensification of the westerlies increased the advection of heat onto the shelf by 160%. Modifying only the winds also enhanced (by 93%) the total heat lost through the surface (either to the atmosphere or melting ice shelves), the heat advected into the ice shelf cavities (by 69%), and the heat lost through the ocean surface underneath the ice shelves (72%: the cause of the increased basal melting in the **Winds** simulation compared to the **Base**). In contrast, increased precipitation produced small decreases in the heat advected onto the shelf and lost through the surface (−7% in both simulations). However, increasing the precipitation led to small increases in the heat advected into the ice shelf cavities (6%) and lost through the ocean/ice shelf interface (3%) compared to only changing the winds. Increased air temperature reduced the net heat advected onto the shelf and lost through the surface (∼−18% in both simulations), but increased the heat advection (30%) and surface heat loss (24%) in the ice shelf cavities compared to the **Winds and Precip** simulation. The net effect of the combined atmospheric forcing changes was to double the heat advected onto the shelf, increase the heat lost through the surface by 50%, and to more than double the heat advected into the ice shelf cavities and lost from the ocean surface into the ice shelf. All three atmospheric changes contributed to increased ice shelf melt.

3.3. Sea Ice and Mixed Layer Depth

Increasing and shifting the winds southward reduced sea ice during summer months that correspond to the phytoplankton growing season (Table 5) in several locations (Figure 3, Figure S4, Tables S3 and S4 in Supporting Information S1), including the Weddell Sea and most of the East Antarctic continental shelf. Increased precipitation led to slight increases in the summer sea ice extent, while increased air temperature further significantly reduced the sea ice concentration in all summer months around the entire continent. Modifying the winds deepened the summer mixed layer (defined by a density change of 0.01 kg m^{-3} relative to the surface value) in all areas

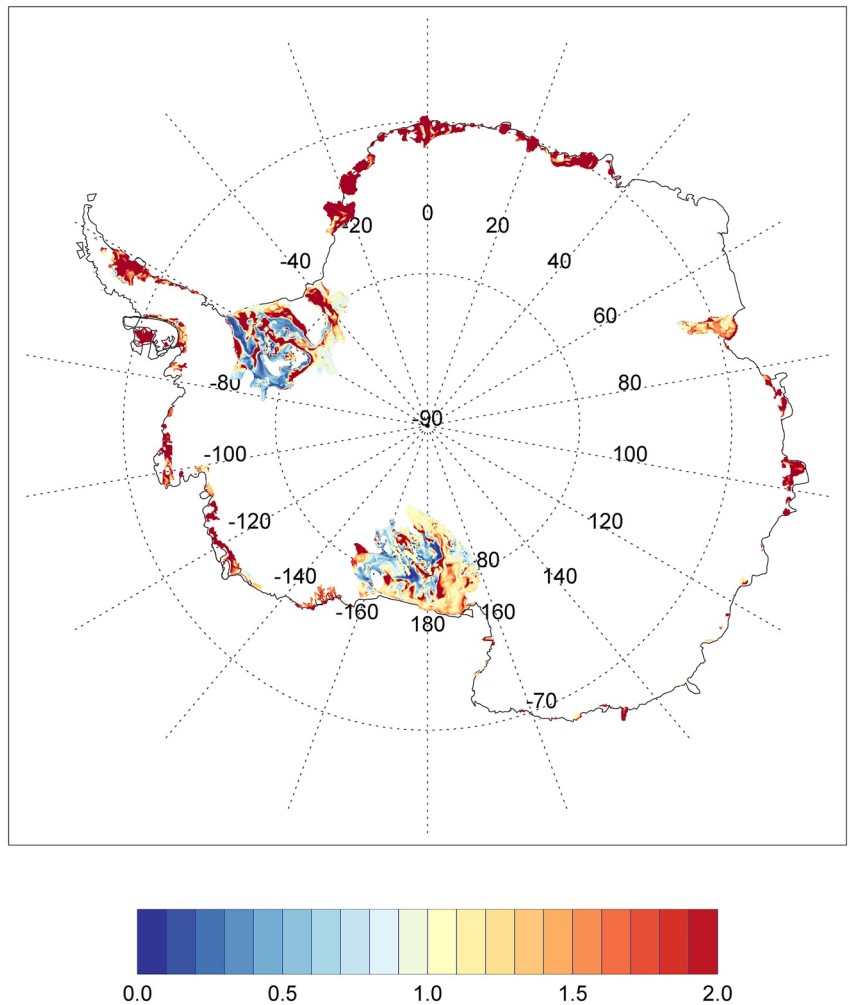

Figure 2. Ratio of mean ice shelf basal melt between the **All** and **Base** simulations.

(Table 6). Increased precipitation led to a slight shoaling of the summer mixed layer, while increased air temperature shoaled the mean mixed layer depth sufficiently, especially in the eastern Amundsen Sea, to overcome the increases due to the wind changes. The resultant mixed layer depths were shallower than those obtained with the unmodified atmospheric forcing fields (**Base** simulation).

3.4. Surface Layer dFe Supply

The average dFe concentration associated with the individual tracers over the ice shelf free surface layer (defined by the top vertical layer of the model) of the Antarctic continental shelf increased over the first 5 years of the

Table 4
Heat Advection Into or Heat Lost Through the Top Surface of Two Bounded Areas (Entire Antarctic Continental Shelf as Defined by the 1,000-m Isobath or Antarctic Ice Shelf Cavities) Over the Last 2 Years of the Four Simulations

Heat quantity	Base TW (10^{12} W)	Winds TW (10^{12} W)	Winds and precip TW (10^{12} W)	All TW (10^{12} W)
Heat advection: continental shelf	57 ± 32	149 ± 48	139 ± 48	114 ± 42
Surface heat lost: continental shelf	−96 ± 124	−185 ± 187	−174 ± 177	−144 ± 217
Heat advection: ice shelf cavities	7.4 ± 7.7	12.5 ± 12.4	13.3 ± 12.6	17.3 ± 17.3
Surface heat lost: ice shelf cavities	−8.9 ± 3.4	−15.3 ± 4.8	−15.8 ± 4.8	−19.6 ± 8.3

Note. Positive values indicate the addition of heat to the volume. The range is the standard deviation of the 5-day averages, which mostly reflects seasonal variability.

Table 5
Sea Ice Area (10^6 km^2) Over the Antarctic Continental Shelf Over the Entire Simulation Period of the Four Simulations for Austral Summer Months That Correspond to the Phytoplankton Growing Season

Time period	Base (10^6 km^2)	Winds (10^6 km^2)	Winds and precip (10^6 km^2)	All (10^6 km^2)
December	1.813	1.286	1.328	1.038
January	1.132	0.770	0.798	0.473
February	0.875	0.581	0.610	0.350
Summer	1.288	0.889	0.922	0.627

Base simulation (Figure S1 in Supporting Information S1). The decrease in surface dFe from biological uptake started in December of the 5th year and extended into the summer (Figure S1 in Supporting Information S1). The time evolution over the last 2 years of the simulation showed the resupply of dFe to the surface layer from the different dFe sources after the initial summer drawdown, the drawdown to near zero during the next summer (and early summer supply from sea ice melt), and the subsequent resupply (Figure S5 in Supporting Information S1). The sediment (39%: i.e., 0.086/0.222) and CDW (32%) sources were the largest suppliers of dFe averaged over the continental shelf surface ocean for the **Base** simulation (Table 7), while sea ice (23%) and ice shelf melt (6%) were still significant sources. Limiting the sediment and CDW dFe sources within the ice shelf cavities reduced the contributions of these sources by 52% and 34%, respectively (Table 7), and the total dFe contribution was reduced by 32% (38% when the direct ice shelf melt contribution was also removed).

The total dFe supply to the surface increased by 53% in the modified wind simulation (Table 7). Most of this increase was due to a large (206%) rise in the sediment contribution to the total dFe supply. The dFe supply was further enhanced by smaller increases in the CDW (51%) and ice shelf melt (9%) sources. The sea ice melt contribution was decreased (−24%). The reduction in total dFe when the ice shelf contributions are removed was lowered to 33% from 38%, indicating a relative decrease in the importance of the ice shelf melt driven overturning contribution. Increased precipitation produced a small (3%) reduction in the total dFe supply. Increased air temperature resulted in a small (6%) rise in the total dFe supply with small decreases in sediment (−7%) and CDW (−6%) sources and increases in the still relatively less important sea ice (78%) and ice shelf (71%) melt sources. The net effect of the three modified atmospheric forcing fields was a 62% increase (+0.138 nM) in total dFe supply relative to that obtained with the unmodified forcing (**All** vs. **Base** simulation, Table 7, Figure 4). This change was driven by a large increase in sediment dFe supply (90%, +0.077 nM), as well as increases in the dFe sources from CDW (43%, +0.031 nM), sea ice melt (36%, 0.018 nM), and ice shelf melt (86%, +0.012 nM).

The modifications to the atmospheric forcing are zonally uniform, but the changes in the dFe supply are regionally heterogeneous (Figure 5). The ratio of the horizontal distribution of the total surface dFe concentration over the Antarctic continental shelf prior to the second bloom season obtained using the modified wind forcing (**Wind** simulation) compared to the unmodified forcing (**Base** simulation) showed as much as a doubling of the dFe supply over much of the East Antarctic continental shelf, the eastern Amundsen Sea, and along the west side of the Antarctic Peninsula (Figure S6 in Supporting Information S1). The surface dFe supply produced using the three atmospheric modifications (**All** simulation) increased by as much as 100% over most of the Antarctic continental shelf except for the large cold water continental shelves in front of the Ronne-Filchner and Ross Ice Shelves (Figure 5). The large decrease in surface dFe supply in the western Weddell Sea was due to a decrease in the sediment supply that only occurred after the atmospheric temperatures were increased (Figure 5 vs. Figure S6 in Supporting Information S1). The ice shelf related fraction of total dFe supply ((Total dFe − ΣdFe_{X_ZC})/Total dFe, Dinniman et al. (2020)) exceeded 0.5 throughout the continental shelf areas of the Amundsen, Bellingshausen, and Weddell Seas (Figure 6a). Imposition of the three modified atmospheric forcing fields did not significantly change the spatial distribution of the portion of the dFe supply provided by ice shelf cavities relative to the **Base** simulation (Figure 6b vs. Figure 6a). However, the relative contribution of dFe from ice shelves in the Amundsen and Bellingshausen Seas, which is mostly due to the ice shelf overturning circulation, increased (Figure S7 in Supporting Information S1).

In the eastern Amundsen Sea, the simulated sediment supply contributed 60% of the total dFe supply for the unmodified atmospheric forcing simulation (**Base**, Table S1 in Supporting Information S1), with 75% of this supply ((0.179–0.044 nM/0.179 nM): Table S1 in Supporting Information S1) first advected into an ice shelf cavity before delivery to the surface waters. The modified wind forcing increased the total dFe supply by 87%, with almost all the change due to increased sediment supply (135% increase). The total dFe supply was decreased by 14% by the addition of increased precipitation with most of this reduction related to decreased sediment supply (22%). The addition of increased atmospheric temperature elevated the dFe supply from CDW, ice shelf melt, and sea ice melt by 27%, 64%, and 143%, respectively, which were partially offset by a 13% decrease in sediment dFe supply resulting in an overall 10% increase in dFe input. The net result of the combined effect of

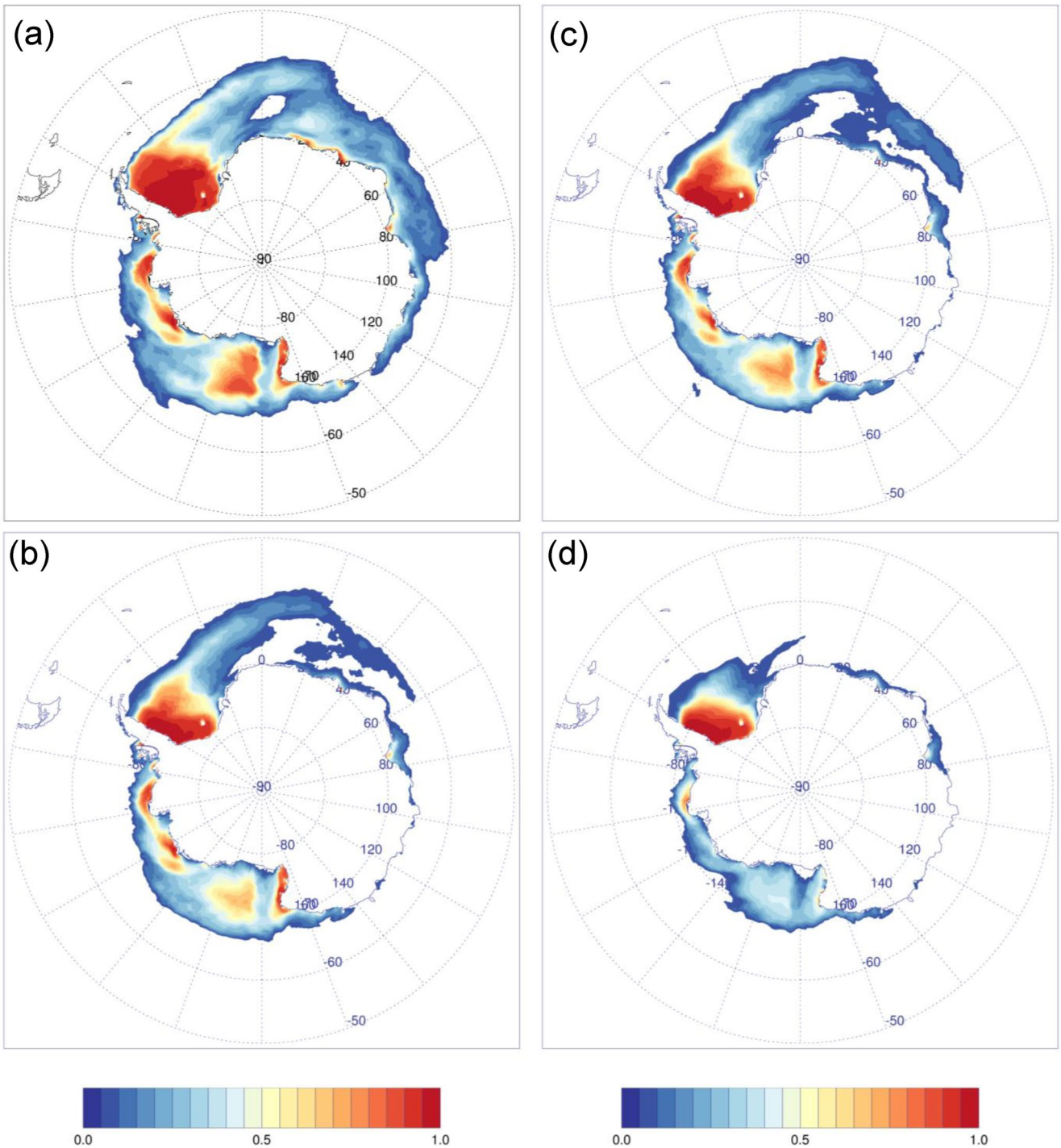

Figure 3. Mean summer (DJF) sea ice concentration for the **Base** (a), **Winds** (b), **Winds + Precip** (c), and **All** (d) simulations. No sea ice is plotted for concentrations below 0.05.

the modified atmospheric forcing for the eastern Amundsen Sea was a 76% increase in the total dFe supply, with significant increases (60%–128%) in each of the four components. The total dFe supply that is due to ice shelf cavities increased from 74% to 78%.

The dFe supply in the open western Ross Sea for unmodified atmospheric conditions was primarily contributed by sediment (38% of the total, Table S2 in Supporting Information S1), CDW (32%), and sea ice (28%)

Table 6
Mean Mixed Layer Depth (m) Over the Entire Simulation Period for December–February (Phytoplankton Growing Season) of the Four Simulations

Location	Base	Winds	Winds and precip	All
Entire open continental shelf	19.4 ± 18.4	26.7 ± 24.4	25.0 ± 22.7	15.1 ± 12.6
Western Ross Sea	14.9 ± 17.2	15.6 ± 19.0	14.8 ± 17.7	10.6 ± 13.6
Eastern Amundsen Sea	29.9 ± 38.3	43.8 ± 65.4	39.3 ± 58.2	9.8 ± 9.1

sources. Only 20% of the total dFe contributions were due to the ice shelf cavity, either directly (ice shelf melt) or indirectly (transiting through the ice shelf cavity). Modifying the winds increased the total dFe supply by only 10% and the addition of increased precipitation decreased the dFe supply by 4%. The elevated atmospheric temperature increased the sea ice and ice shelf melt contributions to the total dFe supply by 52% and 49%, respectively, but made very minor changes to the sediment and CDW sources. The net effect was an overall increase in dFe supply of 15%. The net effect of the combined modifications to the atmospheric forcing for the western Ross Sea was a 22% increase in the total dFe supply. The increases with modified forcing in the contributions from sediment sources (11%) and CDW (8%) were smaller relative to those from sea ice melt (49%) and ice shelf melt (67%). The percentage of the total dFe supply provided by ice shelf cavities remained the same at 20%.

4. Discussion

4.1. Changes in Ice Shelf Basal Melt

Studies with circum-Antarctic or global ocean models that include ice shelves and are forced with projected atmospheric changes show increased basal melting around Antarctica (Kusahara & Hasumi, 2013; Naughten et al., 2018; Timmermann & Hellmer, 2013). The 83% increase in simulated total basal melt rate in this study is similar to the 90% increase obtained from an ocean/sea ice/ice shelf model (Naughten et al., 2018) with similar resolution over the Antarctic continental shelf that was forced for 100 years with CMIP5 RCP8.5 multi-model mean (MMM) atmospheric anomalies added to the same ERA-Interim forcing used in this study. The Naughten et al. (2018) simulations forced with other CMIP5 projections to 2100 showed increases in melt rate ranging from 41% to 129%. Naughten et al. (2018) showed considerable heterogeneity in the melt rate increases, with the RCP8.5 MMM simulation having the smallest relative change in the Ross Sea and the greatest change in the Amundsen Sea, which is similar to results presented here.

Table 7
Modeled dFe Supply Associated With Different Sources From the Four Simulations

Symbol (see Table 1)	dFe source	Base (nM)	Winds (nM)	Winds + precip (nM)	All (nM)
ΣdFe_{ISX}	Ice shelf melt (Sum over all sectors)	0.014	0.015	0.017	0.026
dFe_{SED}	Sediments	0.086	0.176	0.168	0.163
dFe_{SED_ZC}	Sediments	0.041	0.114	0.105	0.096
dFe_{CDW}	Circumpolar Deep Water	0.072	0.109	0.104	0.103
dFe_{CDW_ZC}	Circumpolar Deep Water	0.047	0.077	0.072	0.066
dFe_{SI}	Sea ice melt	0.050	0.038	0.038	0.068
dFe_{SI_ZC}	Sea ice melt	0.049	0.038	0.037	0.067
ΣdFe_{X}	Total supply	0.222	0.339	0.327	0.360
$\Sigma dFe_{X\_ZC} + \Sigma dFe_{ISX}$	Total supply without ice shelf cavity overturning contributions	0.151	0.244	0.231	0.255
ΣdFe_{X_ZC}	Total supply without ice shelf cavity overturning and ice shelf melt contributions	0.137	0.228	0.214	0.229

Note. The dFe concentrations are estimated from the average over the top model layer of the open (not underneath an ice shelf) Antarctic continental shelf for the time between the summer minimum following implementation of biological drawdown and the maximum value prior to the start of summer in the following year (or during the following summer for sea ice melt). The dFe concentrations are obtained by scaling the simulated tracer concentrations by the end member dFe concentrations for each source (see text).

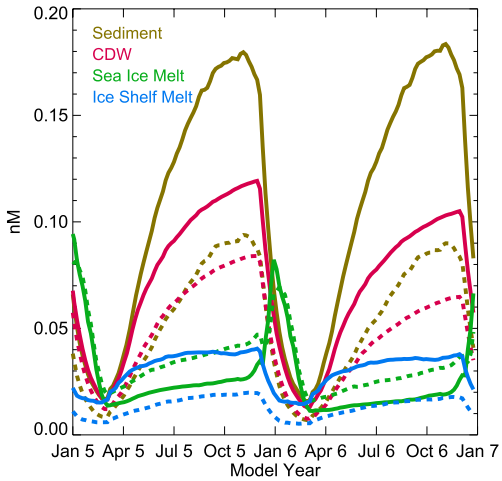

Figure 4. Simulated time evolution of the average surface dFe concentration over the open shelf for the **All** (solid lines) and **Base** (dashed lines) simulations in the last 2 years after implementation of biological uptake.

Increased intensity and a poleward shift in the westerlies have been shown to enhance advection of heat onto the Antarctic continental shelf (e.g., Kusahara & Hasumi, 2013; Naughten et al., 2018; Spence et al., 2014). In this study, the simulation with the modified winds produced an increase in the advective heat input onto the continental shelf of 92 TW, which is the largest incremental increase in heat advection onto the shelf of all the individual modifications to the atmospheric forcing. Because of a possible non-linear response to the incremental forcing changes, the increase in heat advected onto the shelf could be different if the wind change was applied after the other atmospheric changes. However, the results from this study show clearly that changes in wind forcing produce the largest effect on basal melt rate (+50% vs. +1% or +21%) and heat supply to Antarctic shelf waters. The relative importance of the wind changes should be maintained independent of the order in which the incremental atmospheric forcings are applied.

The increased on-shelf heat advection was almost balanced by increased surface heat loss (89 TW) to either the atmosphere, sea ice, or ice shelf. Some of the increased surface heat loss resulted from changes in vertical mixing from increased mechanical wind forcing. However, other processes contributed to the increased surface heat loss (e.g., increased

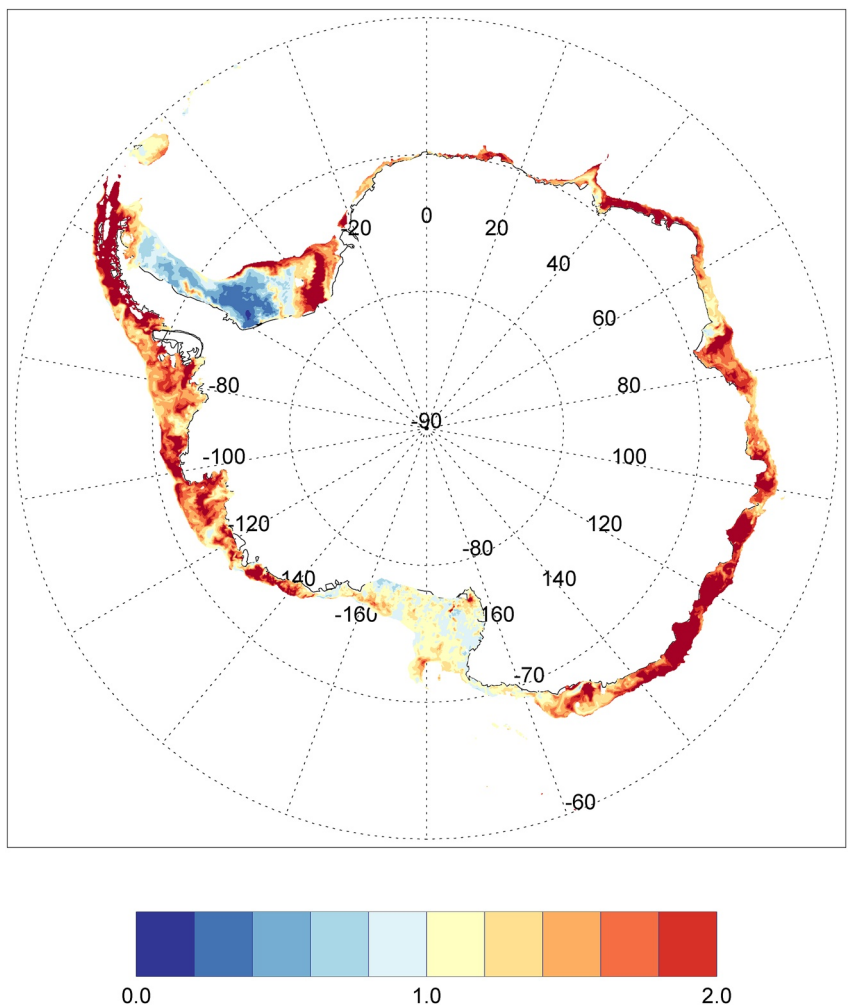

Figure 5. Ratio of the simulated surface layer total dFe concentration just prior to the second bloom season (November of simulation year 5) between the **All** and **Base** simulations.

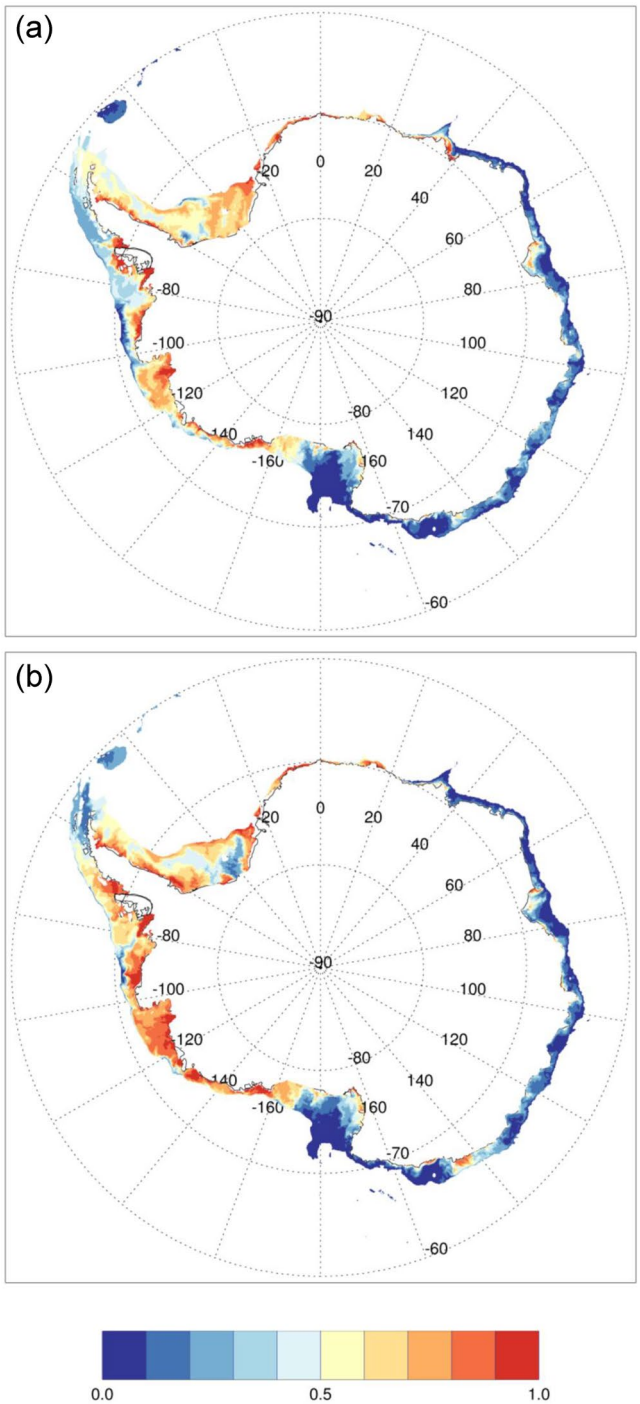

Figure 6. Simulated fraction of ice shelf related dFe to total dFe supply to the surface just prior to the second bloom season for the **Base** (a) and **All** (b) simulations.

sea ice formation and brine rejection, increased ice shelf melting) since much of the West Antarctic continental shelf is south of 70°S where the winds were unchanged. Previous modeling studies (e.g., Dinniman et al., 2015; Naughten et al., 2018; Timmermann & Hellmer, 2013) showed that increased on-shelf advection of warm CDW can be overwhelmed by changes in the conditions over the continental shelf with respect to heat delivery to the ice shelf cavities. However, the modified wind forcing also produced the largest incremental increase in the amount of heat advected into the ice shelf cavities and the heat lost in melting the base of the ice shelves.

The CMIP6 high emissions projections have a less dramatic change in the southern hemisphere westerlies than was used in this study. Goyal et al. (2021) showed that the CMIP6 historical simulations generally better represent the present day position of the westerlies than CMIP5. The ensemble CMIP6 projected mean westerlies at the end of the 21st Century under the high emissions scenario (SSP585 for CMIP6) increase in strength by 10% and shift poleward by ~1°. It is reasonable to assume that if the wind modification used here was reduced in strength and position to the Goyal et al. (2021) estimated changes, then there would be less heat advected onto the continental shelf and into the ice shelf cavities. Thus, the results from this study likely provide an upper estimate for heat advection resulting from modified wind forcing.

4.2. Changes in Importance of Glacial Ice to dFe Supply

For unmodified atmospheric conditions, the ice shelf melt driven overturning was responsible for 32% of the total dFe supply to the surface waters, while the direct contribution from ice shelf melt was only 6%. Implementation of all the atmospheric changes increased the total ice shelf basal melt and the ice shelf direct and indirect contributions to the total dFe supply increased. However, the relative importance of the ice shelf overturning on the total dFe supply decreased to 29% of the total supply.

Dinniman et al. (2020) showed that the fraction of the total supply of dFe due to ice shelves is large in the Amundsen and Bellingshausen Seas (see also Figure 7d in Person et al., 2019), which are known to have reduced vertical mixing on the shelf and high rates of ice shelf basal melt (Jenkins et al., 2016; Petty et al., 2013). For the Ross Sea and much of the East Antarctic continental shelf, contributions of dFe due to ice shelves were small (with the exception of the Weddell Sea), because these shelf systems experience deep winter vertical mixing and low rates of ice shelf basal melt (Dinniman et al., 2020). The simulations with projected changes in atmospheric forcing retained this general pattern of ice shelf contributions to dFe, but the ice shelf melt and overturning contributions increased in the Amundsen and Bellingshausen Seas and became less important in areas where it already was not a primary contributor to dFe, such as much of East Antarctica (Figure S7 in Supporting Information S1). For example, in the eastern Amundsen Sea, the already high percentage of the dFe supply due to ice shelf processes (59% due to overturning and 15% due to ice shelf melt) increases when all the atmospheric changes are imposed (62% and 16%, respectively). The projected changes in atmospheric forcing serve to enhance the heterogeneity of dFe supply to Antarctic continental shelf waters, implying increased heterogeneity in biological production.

4.3. Implications for Changes in Primary Production

Projections based on CMIP5 models show global reductions in primary and export production that are partially compensated for by increases in primary production in high latitudes (Cabré et al., 2014). This increase at high latitudes results from the combined effect of the greater availability of light and dFe to surface waters. Most CMIP5 model simulations show increased light reaching the ocean surface south of 65°S due to accelerated melting of sea ice, even with a concurrent cloud cover increase (Leung et al., 2015). Also, many of the CMIP5 models project enhanced summertime stratification (Hauck et al., 2015; Leung et al., 2015) and increased dFe input in the Southern Ocean over the 21st century (Cabré et al., 2014), even though atmospheric dust deposition is kept constant in the CMIP5 simulations (Leung et al., 2015). However, in many of the models, increased dFe did not correlate with increased production in the high latitude Southern Ocean, suggesting that removal of light limitation may be more important for increasing primary production across the models (Cabré et al., 2014). Other analyses suggested that the increased production resulted from projected increases in nutrients (Hauck et al., 2015). In most CMIP6 models, the present-day total global net primary production is closer to satellite derived estimates than their CMIP5 predecessors (Séférian et al., 2020), but simulated geographical distributions of present-day mean state surface chlorophyll concentrations are only moderately improved (Kwiatkowski et al., 2020). The CMIP6 projections still retain increased primary production at high latitudes for all emissions scenarios that is partially attributed to enhanced stratification that reduces light stress (Kwiatkowski et al., 2020). For the CMIP5 and CMIP6 simulations, the projected increase in primary production was the result of reductions in light or nutrient stress. However, these projections used models that did not explicitly include ice shelves and associated dFe delivery to surface waters.

In this analysis, the simulation that used the combined modified atmospheric forcing fields showed a 43% reduction in sea ice cover, shallowing of summer mixed layer depth (22%), and significant increases in the dFe supply (62%) to the surface waters over the open Antarctic continental shelf. These results are similar to the CMIP5 and CMIP6 projections in that the projected changes have the potential to relieve both light and nutrient limitation during the summer growing season. Increased open water and shallower mixed layer depths increase mean irradiance within the summer mixed layer and the increased dFe supply provides relief from micronutrient limitation in many shelf areas during summer. As a result, the combined effect of increased light and dFe supply can increase the magnitude and length of the growing season for shelf phytoplankton blooms. However, the heterogeneity of the modified shelf water characteristics and dFe supply provides regional variability in the response of phytoplankton growth. For example, the simulations showed larger magnitude changes in summer sea ice area, summer mixed layer depth, and surface dFe supply in the eastern Amundsen Sea than in the Western Ross Sea. This regional variability would be difficult to simulate in a coarser resolution model that did not include the spatially (and temporally on decadal time scales) varying impact of ice shelf melt overturning on nutrient supply. The heterogeneity seen in the simulations underlies a spatially varying productivity that potentially favors increased phytoplankton biomass and production in the eastern Amundsen Sea, with implications for the regional food web.

4.4. Missing dFe Sources

The specification of dFe sources used in this study does not account for inputs from aeolian deposition (Duprat et al., 2019), hydrothermal vents (Ardyna et al., 2019; Schine et al., 2021; Tagliabue & Resing, 2016; Tagliabue, 2014), and glacial meltwater from icebergs and the grounded ice sheet. As discussed in Dinniman et al. (2020), most of these sources are unlikely to be significant at the scale of the entire Antarctic continental shelf. However, Death et al. (2014) used a modeling study to suggest that subglacial meltwater could be a significant additional source of dFe to the broader Southern Ocean, and especially the Antarctic continental shelf. The Death et al. (2014) analysis relied on a wide range of end member concentration values of dFe in the subglacial meltwater, a model estimate of the subglacial meltwater from the Antarctic Ice Sheet, and the assumption that all the subglacial melt is released at the surface of the ocean adjacent to the coast rather than via ice shelf cavities. There are now a few measurements of dFe concentration from subglacial lakes (i.e., Hawkings et al., 2020; Vick-Majors et al., 2020), but these estimates differ by up to three orders of magnitude, suggesting that the endmember concentration of subglacial meltwater dFe remains to be constrained. Also, the total subglacial melt and the flux of this melt across the grounding line are still not well known (e.g., de Flurian et al., 2018) and reasonable future projections of these values remain to be done (Seroussi et al., 2020; Sun et al., 2020). The mechanisms by which the subglacial flux crosses the grounding line and is entrained in the ice shelf basal melt

water plume and exported out of the ice shelf cavity is still a subject of active investigation (i.e., Jenkins, 2011; Cenedese & Gatto, 2016, Hewitt, 2020, Nakayama et al., 2021).

The simple scavenging parameterization used in this study was developed for open ocean systems (Dutkiewicz et al., 2005) and may underestimate scavenging rates on continental shelf systems. This parameterization does not account for availability of particles, which can be present in high concentrations in shelf systems and can undergo substantial seasonal variability in response to phytoplankton growth or sediment resuspension, potentially altering scavenging and dFe supply. Also, the approach used in this study for specifying dFe assumes that iron is bound to a ligand and remains bioavailable in dissolved form. Recent studies suggest a more complex pathway in which dFe is in equilibrium with the labile particulate Fe pool that acts as a buffer when dFe is low (van Manen et al., 2022). This highlights the important role of remineralization of particulate pools in maintaining dFe concentrations (Gerringa et al., 2020) which is also not explicitly represented in our simulations. Another example of the contribution of particulate Fe is that although dFe is often released in the initial stages of sea ice melt, the dissolution of particles becomes a source of Fe later in the season (e.g., Lannuzel et al., 2010, their Figure 6).

5. Conclusions

The projected changes in the atmospheric conditions in 2100 will have important effects on Antarctic continental shelf systems. Ice shelves will be exposed to warmer waters, due more to strengthening and poleward shifting winds rather than increases in precipitation or atmospheric temperatures, leading to enhanced basal melting with unknown implications for ice shelf stability. Increased ice shelf melt will enhance freshwater input to the continental shelf, with consequent effects on stratification and circulation. Enhanced ice shelf basal melting will also increase the strength of the ice cavity overturning circulation, thereby increasing delivery of dFe to continental shelf surface waters. This increased dFe delivery has the potential to increase biological production of the Antarctic shelf systems. The heterogeneity in regional response to increased dFe supply has important implications for regional production. Continued refinement of regional circulation models that include biogeochemical components will be needed to address questions of projected effects on regional biological production.

The results from this study point to the importance of understanding the balance between increased summer irradiance, due to both reduced summer sea ice and shallower summer mixed layers, and greater dFe availability over the surface waters of the Antarctic continental shelf on annual production, similar to results from CMIP5 and CMIP6 projections. Much of the observed heterogeneity (Arrigo et al., 2008, 2015; Sullivan et al., 1993) in surface phytoplankton may be due to differences in the melting of and circulation driven by ice shelves, and this spatial variability could increase in the future. Current efforts to add ice shelf processes to fully coupled Earth System Models are focused on the physical response of the climate system to land ice/ocean interactions. However, there will be important biogeochemical interactions as well, likely impacting phytoplankton as well as higher trophic level organisms that depend on phytoplankton as a food source. As Earth System Models strive to improve their modeling of the ocean ecosystem, it will be important to include not only sea ice, but the ocean interactions with the land based component of the cryosphere as well.

Data Availability Statement

The circulation model data (including all simulated tracers) used for this analysis is available at BCO-DMO at https://www.bco-dmo.org/dataset/887777.

Acknowledgments
This research was supported by the National Science Foundation under Grants OPP-1643652 to Old Dominion University, OPP-1643618 to Stanford University, OPP-1941292 to VIMS, and by the Wahab High Performance Computing cluster at Old Dominion University. Comments from four reviewers considerably improved the manuscript.

References

Adler, R. F., Huffman, G. J., Chang, A., Ferraro, R., Xie, P. P., Janowiak, J., et al. (2003). The version-2 global precipitation climatology project (GPCP) monthly precipitation analysis (1979-present). *Journal of Hydrometeorology*, *4*(6), 1147–1167. https://doi.org/10.1175/1525-7541(2003)004<1147:TVGPCP>2.0.CO;2

Adusumilli, S., Fricker, H. A., Medley, B., Padman, L., & Siegfried, M. R. (2020). Interannual variations in meltwater input to the Southern Ocean from Antarctic ice shelves. *Nature Geoscience*, *13*(9), 616–620. https://doi.org/10.1038/s41561-020-0616-z

Ardyna, M., Lacour, L., Sergi, S., d'Ovidio, F., Sallée, J. B., Rembauville, M., et al. (2019). Hydrothermal vents trigger massive phytoplankton blooms in the Southern Ocean. *Nature Communications*, *10*(1), 2451. https://doi.org/10.1038/s41467-019-09973-6

Arrigo, K. R., DiTullio, G. R., Dunbar, R. B., Robinson, D. H., VanWoert, M., Worthen, D. L., & Lizotte, M. P. (2000). Phytoplankton taxonomic variability and nutrient utilization and primary production in the Ross Sea. *Journal of Geophysical Research*, *105*(C4), 8827–8846. https://doi.org/10.1029/1998jc000289

Arrigo, K. R., van Dijken, G. L., & Bushinsky, S. (2008). Primary production in the Southern Ocean, 1997–2006. *Journal of Geophysical Research*, *113*(C8), C08004. https://doi.org/10.1029/2007JC004551

Arrigo, K. R., van Dijken, G. L., & Strong, A. L. (2015). Environmental controls of marine productivity hot spots around Antarctica. *Journal of Geophysical Research*, *120*(8), 5545–5565. https://doi.org/10.1002/2015JC010888

Barthel, A., Agosta, C., Little, C. M., Hattermann, T., Jourdain, N. C., Goelzer, H., et al. (2020). CIMP5 model section for ISMIP6 ice sheet model forcing: Greenland and Antarctica. *The Cryosphere*, *14*(3), 855–879. https://doi.org/10.5194/tc-14-855-2020

Behrangi, A., & Richardson, M. (2018). Observed high-latitude precipitation amount and pattern and CMIP5 model projections. *Remote Sensing*, *10*, 1583. https://doi.org/10.3390/rs10101583

Biddle, L., Heywood, K., Kaiser, J., & Jenkins, A. (2017). Glacial meltwater identification in the Amundsen Sea. *Journal of Physical Oceanography*, *47*(4), 933–954. https://doi.org/10.1175/JPO-D-16-0221.1

Biddle, L. C., Loose, B., & Heywood, K. J. (2019). Upper ocean distribution of glacial meltwater in the Amundsen Sea, Antarctica. *Journal of Geophysical Research*, *124*(10), 6854–6870. https://doi.org/10.1002/2019JC015133

Boyd, P. W. (2002). Environmental factors controlling phytoplankton processes in the Southern Ocean. *Journal of Phycology*, *38*(5), 844–861. https://doi.org/10.1046/j.1529-8817.2002.t01-1-01203.x

Boyd, P. W., Arrigo, K. R., Strzepek, R., & van Dijken, G. L. (2012). Mapping phytoplankton iron utilization: Insights into Southern Ocean supply mechanisms. *Journal of Geophysical Research*, *117*(C6), C06009. https://doi.org/10.1029/2011JC007726

Bracegirdle, T. J., Hyder, P., & Holmes, C. R. (2018). CMIP5 diversity in Southern westerly jet projections related to historical sea ice area: Strong link to strengthening and weak link to shift. *Journal of Climate*, *31*(1), 195–211. https://doi.org/10.1175/JCLI-D-17-0320.1

Bronselaer, B., Russell, J. L., Winton, M., Williams, N. L., Key, R. M., Dunne, J. P., et al. (2020). Importance of wind and meltwater for observed chemical and physical changes in the Southern Ocean. *Nature Geoscience*, *13*(1), 35–42. https://doi.org/10.1038/s41561-019-0502-8

Budgell, P. (2005). Numerical simulation of ice-ocean variability in the Barents Sea region towards dynamical downscaling. *Ocean Dynamics*, *55*(3–4), 370–387. https://doi.org/10.1007/s10236-005-0008-3

Cabré, A., Marinov, I., & Leung, S. (2014). Consistent global responses of marine ecosystems to future climate change across the IPCC AR5 Earth system models. *Climate Dynamics*, *45*(5–6), 1253–1280. https://doi.org/10.1007/s00382-014-2374-3

Carton, J. A., & Giese, B. A. (2008). A reanalysis of ocean climate using SODA. *Monthly Weather Review*, *136*(8), 2999–3017. https://doi.org/10.1175/2007MWR1978.1

Cenedese, C., & Gatto, V. M. (2016). Impact of a localized source of subglacial discharge on the heat flux and submarine melting of a tidewater glacier: A laboratory study. *Journal of Physical Oceanography*, *46*(10), 3155–3163. https://doi.org/10.1175/JPO-D-16-0123.1

Death, R., Wadham, J. L., Monteiro, F., Le Brocq, A. M., Tranter, M., Ridgwell, A., et al. (2014). Antarctic ice sheet fertilises the Southern Ocean. *Biogeosciences*, *11*(10), 2635–2644. https://doi.org/10.5194/bg-11-2635-2014

DeBaar, H. J. W., Buma, A. G. J., Nolting, R. F., Cadee, G. C., Jacques, G., & Treguer, P. J. (1990). On iron limitation of the Southern Ocean: Experimental observations in the Weddell and Scotia Sea. *Marine Ecology Progress Series*, *65*, 105–122. https://doi.org/10.3354/meps065105

Dee, D. P., Uppala, S. M., Simmons, A. J., Berrisford, P., Poli, P., Kobayashi, S., et al. (2011). The ERA-Interim reanalysis: Configuration and performance of the data assimilation system. *Quarterly Journal of the Royal Meteorological Society*, *137*(656), 553–597. https://doi.org/10.1002/qj.828

de Flurian, B., Werder, M. A., Beyer, S., Brinkerhoff, D. J., Delaney, I., Dow, C. F., et al. (2018). SHMIP the subglacial hydrology model intercomparison Project. *Journal of Glaciology*, *64*(248), 897–916. https://doi.org/10.1017/jog.2018.78

Depoorter, M. A., Bamber, J. L., Griggs, J. A., Lenaerts, J. T. M., Ligtenberg, S. R. M., van den Broeke, M. R., & Moholdt, G. (2013). Calving fluxes and basal melt rates of Antarctic ice shelves. *Nature*, *502*(7469), 89–92. https://doi.org/10.1038/nature12567

Dinniman, M. S., Kinck, J. M., Bai, L.-S., Bromwich, D. H., Hines, K. M., & Holland, D. M. (2015). The effect of atmospheric forcing resolution on delivery of ocean heat to the Antarctic floating ice shelves. *Journal of Climate*, *28*(15), 6067–6085. https://doi.org/10.1175/JCLI-D-14-00374.1

Dinniman, M. S., Klinck, J. M., Hofmann, E. E., & Smith, W. O., Jr. (2018). Effect of projected changes in wind, atmospheric temperature, and freshwater inflow on the Ross Sea. *Journal of Climate*, *31*(4), 1619–1635. https://doi.org/10.1175/JCLI-D-17-0351.1

Dinniman, M. S., Klinck, J. M., & Smith, W. O., Jr. (2011). A model study of Circumpolar Deep Water on the West Antarctic Peninsula and Ross Sea continental shelves. *Deep Sea Res. II*, *58*(13–16), 1508–1523. https://doi.org/10.1016/j.dsr2.2010.11.013

Dinniman, M. S., St-Laurent, P., Arrigo, K. R., Hofmann, E. E., & van Dijken, G. L. (2020). Analysis of iron sources in Antarctic continental shelf waters. *Journal of Geophysical Research*, *125*(5), e2019JC015736. https://doi.org/10.1029/2019JC015736

Donat-Magnin, M., Jourdain, N. C., Spence, P., Le Sommer, J., Gallée, H., & Durand, G. (2017). Ice-shelf melt response to changing winds and glacier dynamics in the Amundsen Sea Sector, Antarctica. *Journal of Geophysical Research*, *122*(12), 10206–10224. https://doi.org/10.1002/2017JC013059

Duprat, L., Kanna, N., Janssens, J., Roukaerts, A., Deman, F., Townsend, A. T., et al. (2019). Enhanced iron flux to Antarctic sea ice via dust deposition from ice-free coastal areas. *Journal of Geophysical Research*, *124*(12), 8538–8557. https://doi.org/10.1029/2019JC015221

Dutkiewicz, S., Follows, M. J., & Parekh, P. (2005). Interactions of the iron and phosphorus cycles: A three-dimensional model study. *Global Biogeochemical Cycles*, *19*(1), GB1021. https://doi.org/10.1029/2004GB002342

Forsch, K. O., Hahn-Woernle, L., Sherrell, R. M., Roccanova, V. J., Bu, K., Burdige, D., et al. (2021). Seasonal dispersal of fjord meltwaters as an important source of iron and manganese to coastal Antarctic phytoplankton. *Biogeosciences*, *18*(23), 6349–6375. https://doi.org/10.5194/bg-18-6349-2021

Gerringa, L. J. A., Alderkamp, A., Laan, P., Thuróczy, C., De Baar, H. J. W., Mills, M. M., et al. (2012). Iron from melting glaciers fuels the phytoplankton blooms in Amundsen Sea (Southern Ocean): Iron biogeochemistry. *Deep Sea Research Part II*, *71–76*, 16–31. https://doi.org/10.1016/j.dsr2.2012.03.007

Gerringa, L. J. A., Alderkamp, A., Laan, P., Thuróczy, C., De Baar, H. J. W., Mills, M. M., et al. (2020). Corrigendum to "Iron from melting glaciers fuels the phytoplankton blooms in Amundsen Sea (Southern Ocean): Iron biogeochemistry" (Gerringa et al., 2012). *Deep Sea Research Part II*, *177*, 104843. https://doi.org/10.1016/j.dsr2.2020.104843

Goyal, R., Gupta, A. S., Jucker, M., & England, M. H. (2021). Historical and projected changes in the Southern Hemisphere surface westerlies. *Geophysical Research Letters*, *48*(4), e2020GL090849. https://doi.org/10.1029/2020GL090849

Greisman, P. (1979). On upwelling driven by the melt of ice shelves and tidewater glaciers. *Deep-Sea Researc*h, *26*A(9), 1051–1065. https://doi.org/10.1016/0198-0149(79)90047-5

Haidvogel, D. B., Arango, H., Budgell, W. P., Cornuelle, B. D., Curchitser, E., Di Lorenzo, E., et al. (2008). Ocean forecasting in terrain-following coordinates: Formulation and skill assessment of the Regional Ocean Modeling System. *Journal of Computational Physics*, *227*(7), 3595–3624. https://doi.org/10.1016/j.jcp.2007.06.016

Häkkinen, S., & Mellor, G. L. (1992). Modeling the seasonal variability of a coupled Arctic ice-ocean system. *Journal of Geophysical Research*, *97*(C12), 20285–20304. https://doi.org/10.1029/92jc02037

Hauck, J., Volker, C., Wolf-Gladrow, D. A., Laufkotter, C., Vogt, M., Aumont, O., et al. (2015). On the Southern Ocean CO_2 uptake and the role of the biological carbon pump in the 21st century. *Global Biogeochemical Cycles*, *29*(9), 1451–1470. https://doi.org/10.1002/2015GB005140

Hawkings, J. R., Skidmore, M. L., Wadham, J. L., Priscu, J. C., Morton, P. L., Hatton, J. E., et al. (2020). Enhanced trace element mobilization by Earth's ice sheets. *Proceedings of the National Academy of Sciences*, *117*(50), 31648–31659. https://doi.org/10.1073/pnas.2014378117

Hewitt, I. J. (2020). Subglacial plumes. *Annual Review of Fluid Mechanics*, *52*(1), 145–169. https://doi.org/10.1146/annurev-fluid-010719-060252

Holland, D. M., & Jenkins, A. (1999). Modelling thermodynamic ice-ocean interactions at the base of an ice shelf. *Journal of Physical Oceanography*, *29*(8), 1787–1800. https://doi.org/10.1175/1520-0485(1999)029<1787:mtioia>2.0.co;2

Holland, P. R., & Kwok, R. (2012). Wind-driven trends in Antarctic sea-ice drift. *Nature Geoscience*, *5*(12), 872–875. https://doi.org/10.1038/ngeo1627

Hunke, E. C. (2001). Viscous-plastic sea ice dynamics with the EVP model: Linearization issues. *Journal of Computational Physics*, *170*(1), 18–38. https://doi.org/10.1006/jcph.2001.6710

Hunke, E. C., & Dukowicz, J. K. (1997). An elastic-viscous-plastic model for sea ice dynamics. *Journal of Physical Oceanography*, *27*(9), 1849–1867. https://doi.org/10.1175/1520-0485(1997)027<1849:aevpmf>2.0.co;2

Jenkins, A. (2011). Convection-driven melting near the grounding lines of ice shelves and tidewater glaciers. *Journal of Physical Oceanography*, *41*(12), 2279–2294. https://doi.org/10.1175/JPO-D-11-03.1

Jenkins, A., Dutrieux, P., Jacobs, S., Steig, E. J., Gudmundsson, G. H., Smith, J., & Heywood, K. J. (2016). Decadal ocean forcing and Antarctic ice sheet response: Lessons from the Amundsen Sea. *Oceanography*, *29*(4), 106–117. https://doi.org/10.5670/oceanog.2016.103

Jeong, H., Asay-Davis, X. S., Turner, A. K., Comeau, D. S., Price, S. F., Abernathey, R. P., et al. (2020). Impacts of ice-shelf melting on water-mass transformation in the Southern Ocean from E3SM simulations. *Journal of Climate*, *33*(13), 5787–5807. https://doi.org/10.1175/JCLI-D-19-0683.1

Jourdain, N. C., Mathiot, P., Merino, N., Durand, G., Le Sommer, J., Spence, P., et al. (2017). Ocean circulation and sea-ice thinning induced by melting ice shelves in the Amundsen Sea. *Journal of Geophysical Research*, *122*(3), 2550–2573. https://doi.org/10.1002/2016JC012509

Kusahara, K., & Hasumi, H. (2013). Modeling Antarctic ice shelf responses to future climate changes and impacts on the ocean. *Journal of Geophysical Research*, *118*(5), 2454–2475. https://doi.org/10.1002/j.grc.20166

Kwiatkowski, L., Torres, O., Bopp, L., Aumont, O., Chamberlain, M., Christian, J. R., et al. (2020). Twenty-first century ocean warming, acidification, deoxygenation, and upper-ocean nutrient and primary production decline from CMIP6 model projections. *Biogeosciences*, *17*(13), 3439–3470. https://doi.org/10.5194/bg-17-3439-2020

Lannuzel, D., Schoemann, V., de Jong, J., Pasquer, B., van der Merwe, P., Masson, F., et al. (2010). Distribution of dissolved iron in Antarctic sea ice: Spatial, seasonal, and inter-annual variability. *Journal of Geophysical Research*, *115*(G3), G03022. https://doi.org/10.1029/2009JG001031

Lannuzel, D., Vancoppenolle, M., van der Merwe, P., de Jong, J., Meiners, K. M., Grotti, M., et al. (2016). Iron in sea ice: Review and new insights. *Elementa: Science of the Anthropocene*, *4*(000130), 130. https://doi.org/10.12952/journal.elementa.000130

Laufkötter, C., Stern, A. A., John, J. G., Stock, C. A., & Dunne, J. P. (2018). Glacial iron sources stimulate the Southern Ocean carbon cycle. *Geophysical Research Letters*, *45*(24), 13377–13385. https://doi.org/10.1029/2018GL079797

Leung, S., Cabré, A., & Marinov, I. (2015). A latitudinally banded phytoplankton response to 21st century climate change in the Southern ocean across the CMIP5 model suite. *Biogeosciences*, *12*(19), 5715–5734. https://doi.org/10.5194/bg-12-5715-2015

Liu, Y., Moore, J. C., Cheng, X., Gladstone, R. M., Bassis, J. N., Liu, H., et al. (2015). Ocean-driven thinning enhances iceberg calving and retreat of Antarctic ice shelves. *Proceedings of the National Academy of Sciences*, *112*(11), 3263–3268. https://doi.org/10.1073/pnas.1415137112

Locarnini, R. A., Mishonov, A. V., Antonov, J. I., Boyer, T. P., Garcia, H. E., Baranova, O. K., et al. (2010). Temperature. Volume 1, World Ocean Atlas 2009, NOAA Atlas NESDIS 68 (p. 184).

Mack, S. L., Dinniman, M. S., McGillicuddy, D. J., Jr., Sedwick, P. N., & Klinck, J. M. (2017). Dissolved iron transport pathways in the Ross Sea: Influence of tides and mesoscale eddies in a regional ocean model. *Journal of Marine Systems*, *166*, 73–86. https://doi.org/10.1016/j.marsys.2016.10.008

Mallett, H. K. W., Boehme, L., Fedak, M., Heywood, K. J., Stevens, D. P., & Roquet, F. (2018). Variation in the distribution and properties of circumpolar deep water in the eastern Amundsen Sea, on seasonal timescales, using seal-borne tags. *Geophysical Research Letters*, *45*(10), 4982–4990. https://doi.org/10.1029/2018GL077430

Martin, J. H., Fitzwater, S. E., & Gordon, R. M. (1990). Iron deficiency limits plankton growth in Antarctic waters. *Global Biogeochemical Cycles*, *4*(1), 5–12. https://doi.org/10.1029/gb004i001p00005

McGillicuddy, D. J., Sedwick, P. N., Dinniman, M. S., Arrigo, K. R., Bibby, T. S., Greenan, B. J. W., et al. (2015). Iron supply and demand in an Antarctic shelf ecosystem. *Geophysical Research Letters*, *42*(19), 8088–8097. https://doi.org/10.1002/2015GL065727

Mellor, G. L., & Kantha, L. (1989). An ice-ocean coupled model. *Journal of Geophysical Research*, *94*(C8), 10937–10954. https://doi.org/10.1029/jc094ic08p10937

Millan, R., Rignot, E., Bernier, V., Morlighem, M., & Dutrieux, P. (2017). Bathymetry of the Amundsen Sea Embayment sector of West Antarctica from operation IceBridge gravity and other data. *Geophysical Research Letters*, *44*(3), 1360–1368. https://doi.org/10.1002/2016GL072071

Mills, M. M., Alderkamp, A.-C., Thurcózy, C.-E., van Dijken, G. L., Laan, P., de Baar, H., & Arrigo, K. R. (2012). Phytoplankton biomass and pigment responses to Fe amendments in the Pine Island and Amundsen polynyas. *Deep Sea Research Part II*, *71–76*, 61–76. https://doi.org/10.1016/j.dsr2.2012.03.008

Nakayama, Y., Cai, C., & Seroussi, H. (2021). Impact of subglacial freshwater discharge on pine Island Ice Shelf. *Geophysical Research Letters*, *48*(18), e2021GL093923. https://doi.org/10.1029/2021GL093923

Naughten, K. A., Meissner, K. J., Galton-Fenzi, B. K., England, M. H., Timmermann, R., & Hellmer, H. H. (2018). Future projections of Antarctic ice shelf melting based on CMIP5 scenarios. *Journal of Climate*, *31*(13), 5243–5261. https://doi.org/10.1175/JCLI-D-17-0854.1

Palerme, C., Genthon, C., Claud, C., Kay, J. E., Wood, N. B., & L'Ecuyer, T. (2017). Evaluation of current and projected Antarctic precipitation in CMIP5 models. *Climate Dynamics*, *48*(1–2), 225–239. https://doi.org/10.1007/s00382-016-3071-1

Person, R., Aumont, O., Madec, G., Vancoppenolle, M., Bopp, L., & Merino, N. (2019). Sensitivity of ocean biogeochemistry to the iron supply from the Antarctic Ice Sheet explored with a biogeochemical model. *Biogeosciences*, *16*(18), 3583–3603. https://doi.org/10.5194/bg-16-3583-2019

Person, R., Vancoppenolle, M., Aumont, O., & Malsang, M. (2021). Continental and sea ice iron sources fertilize the Southern Ocean in Synergy. *Geophysical Research Letters*, *48*(23), e2021GL094761. https://doi.org/10.1029/2021GL094761

Petty, A. A., Feltham, D. L., & Holland, P. R. (2013). Impact of atmospheric forcing on Antarctic continental shelf water masses. *Journal of Physical Oceanography*, *43*(5), 920–940. https://doi.org/10.1175/JPO-D-12-0172.1

Petty, A. A., Holland, P. R., & Feltham, D. L. (2014). Sea ice and the ocean mixed layer over the Antarctic shelf seas. *The Cryosphere*, *8*(2), 761–783. https://doi.org/10.5194/tc-8-761-2014

Piñones, A., Hofmann, E. E., Costa, D. P., Goetz, K., Burns, J. M., Roquet, F., et al. (2019). Hydrographic variability along the inner and mid-shelf region of the western Ross Sea obtained using instrumented seals. *Progress in Oceanography*, *174*, 131–142. https://doi.org/10.1016/j.pocean.2019.01.003

Randall-Goodwin, E., Meredith, M. P., Jenkins, A., Yager, P. L., Sherrell, R. M., Abrahamsen, E. P., et al. (2015). Freshwater distribution and water mass structure in the Amundsen Sea Polynya region, Antarctica. *Elementa*, *3*, 65. https://doi.org/10.12952/journal.elementa.000065

Rignot, E., Jacobs, S., Mouginot, J., & Scheuchl, B. (2013). Ice shelf melting around Antarctica. *Science*, *341*(6143), 266–270. https://doi.org/10.1126/science.1235798

Salmon, E., Hofmann, E. E., Dinniman, M. S., & Smith, W. O., Jr. (2020). Evaluation of iron sources in the Ross Sea. *Journal of Marine Systems*, *212*, 103429. https://doi.org/10.1016/j.jmarsys.2020.103429

Schaffer, J., Timmermann, R., Arndt, J. E., Kristensen, S. S., Mayer, C., Morlighem, M., & Steinhage, D. (2016). A global, high-resolution data set of ice sheet topography, cavity geometry, and ocean bathymetry. *Earth System Science Data*, *8*(2), 543–557. https://doi.org/10.5194/essd-8-543-2016

Schine, C. M. S., Alderkamp, A.-C., van Dijken, G., Gerringa, L. J. A., Sergi, S., Laan, P., et al. (2021). Massive Southern Ocean phytoplankton bloom fed by iron of possible hydrothermal origin. *Nature Communications*, *12*(1), 1211. https://doi.org/10.1038/s41467-021-21339-5

Séférian, R., Berthet, S., Yool, A., Palmiéri, J., Bopp, L., Tagliabue, A., et al. (2020). Tracking improvement in simulated marine biogeochemistry between CMIP5 and CMIP6. *Current Climate Change Reports*, *6*(3), 95–119. https://doi.org/10.1007/s40641-020-00160-0

Seroussi, H., Nowicki, S., Payne, A. J., Goelzer, H., Lipscomb, W. H., Abe-Ouchi, A., et al. (2020). ISMIP6 Antarctica: A multi-model ensemble of the Antarctic ice sheet evolution over the 21st century. *The Cryosphere*, *14*(9), 3033–3070. https://doi.org/10.5194/tc-14-3033-2020

Seyitmuhammedov, K., Stirling, C. H., Reid, M. R., van Hale, R., Laan, P., Arrigo, K. R., et al. (2022). The distribution of Fe across the shelf of the Western Antarctic Peninsula at the start of the phytoplankton growing season. *Marine Chemistry*, *238*, 104066. https://doi.org/10.1016/j.marchem.2021.104066

Shchepetkin, A. F., & McWilliams, J. C. (2009). Correction and commentary for "Ocean forecasting in terrain-following coordinate: Formulation and skill assessment of the regional ocean modeling system" by Haidvogel et al., J. Comp. Phys. 227, pp. 3595–3634. *Journal of Computational Physics*, *228*, 8985–9000. https://doi.org/10.1016/j.jcp.2009.09.002

Sherrell, R. M., Lagerström, M. E., Forsch, K. O., Stammerjohn, S. E., & Yager, P. L. (2015). Dynamics of dissolved iron and other bioactive trace metals (Mn, Ni, Cu, Zn) in the Amundsen Sea Polynya, Antarctica. *Elem. Sci. Anthropocene*, *3*, 71. https://doi.org/10.12952/journal.elementa.000071

Simpson, I. R., & Polvani, L. M. (2016). Revisiting the relationship between jet position, forced response, and annular mode variability in the southern midlatitudes. *Geophysical Research Letters*, *43*(6), 2896–2903. https://doi.org/10.1002/2016GL067989

Smith, A. J. R., Ratnarajah, L., Holmes, T. M., Wuttig, K., Townsend, A. T., Westwood, K., et al. (2021). Circumpolar Deep Water and shelf sediments support late summer microbial iron remineralization. *Global Biogeochemical Cycles*, *35*(11), e2020GB006921. https://doi.org/10.1029/2020GB006921

Smith, W. O., & Gordon, L. I. (1997). Hyperproductivity of the Ross Sea (Antarctica) polynya during austral spring. *Geophysical Research Letters*, *24*(3), 233–236. https://doi.org/10.1029/96gl03926

Spence, P., Griffies, S. M., England, M. H., Hogg, A. M. C., Saenko, O. A., & Jourdain, N. C. (2014). Rapid subsurface warming and circulation changes of Antarctic coastal waters by poleward shifting winds. *Geophysical Research Letters*, *41*(13), 4601–4610. https://doi.org/10.1002/2014GL060613

Steele, M., Mellor, G. L., & McPhee, M. G. (1989). Role of the molecular sublayer in the melting or freezing of sea ice. *Journal of Physical Oceanography*, *55*(1), 139–147. https://doi.org/10.1175/1520-0485(1989)019<0139:rotmsi>2.0.co;2

St-Laurent, P., Yager, P. L., Sherrell, R. M., Stammerjohn, S. E., & Dinniman, M. S. (2017). Pathways and supply of dissolved iron in the Amundsen Sea (Antarctica). *Journal of Geophysical Research*, *122*(9), 7135–7162. https://doi.org/10.1002/2017JC013162

Sullivan, C. W., Arrigo, K. R., McClain, C. R., Comiso, J. C., & Firestone, J. (1993). Distributions of phytoplankton blooms in the Southern Ocean. *Science*, *262*(5141), 1832–1837. https://doi.org/10.1126/science.262.5141.1832

Sun, S., Pattyn, F., Simon, E. G., Albrecht, T., Cornford, S., Calov, R., et al. (2020). Antarctic ice sheet response to sudden and sustained ice-shelf collapse (ABUMIP). *Journal of Glaciology*, *66*(260), 891–904. https://doi.org/10.1017/jog.2020.67

Tagliabue, A. (2014). More to hydrothermal iron input than meets the eye. *Proceedings of the National Academy of Sciences*, *111*(47), 16641–16642. https://doi.org/10.1073/pnas.1419829111

Tagliabue, A., & Resing, J. (2016). Impact of hydrothermalism on the ocean iron cycle. *Philosophical Transactions of the Royal Society A*, *374*(2081), 20150291. https://doi.org/10.1098/rsta.2015.0291

Taylor, K. E., Stouffer, R. J., & Meehl, G. A. (2012). An overview of CMIP5 and the experiment design. *Bulletin of the American Meteorological Society*, *93*(4), 485–498. https://doi.org/10.1175/bams-d-11-00094.1

Timmermann, R., & Hellmer, H. H. (2013). Southern Ocean warming and increased ice shelf basal melting in the 21st and 22nd centuries based on coupled ice-ocean finite-element modeling. *Ocean Dynamics*, *63*(9–10), 1011–1026. https://doi.org/10.1007/s10236-013-0642-0

Twelves, A. G., Goldberg, D. N., Henley, S. F., Mazloff, M. R., & Jones, D. C. (2021). Self-shading and meltwater spreading control the transition from light to iron limitation in an Antarctic coastal polynya. *Journal of Geophysical Research*, *126*(2), e2020JC016636. https://doi.org/10.1029/2020JC016636

Van Manen, M., Aoki, S., Brussard, C. P. D., Conway, T. M., Eich, C., Gerringa, L. J. A., et al. (2022). The role of the Dotson ice shelf and circumpolar deep water as driver and source of dissolved and particulate iron and manganese in the Amundsen Sea polynya, Southern Ocean. *Marine Chemistry*, *246*, 104161. https://doi.org/10.1016/j.marchem.2022.104161

Vick-Majors, T. J., Michaud, A. B., Skidmore, M. L., Turetta, C., Barbante, C., Christner, B. C., et al. (2020). Biogeochemical connectivity between freshwater ecosystems beneath the West Antarctic ice sheet and the sub-ice marine environment. *Global Biogeochemical Cycles*, *34*(3), e2019GB006446. https://doi.org/10.1029/2019GB006446

Wilcox, L. J., Charlton-Perez, A. J., & Gray, L. J. (2012). Trends in Austral jet position in ensembles of high- and low-top CMIP5 models. *Journal of Geophysical Research*, *117*(D13), D13115. https://doi.org/10.1029/2012JD017597

Yoon, S. T., Lee, W. S., Stevens, C., Jendersie, S., Nam, S., Yun, S., et al. (2020). Variability in high-salinity shelf water production in the Terra Nova Bay polynya, Antarctica. *Ocean Science*, *16*(2), 373–388. https://doi.org/10.5194/os-16-373-2020